Automotive Science and Engineering, Vol. 16, No. 3, (2026), 5178-5188

Iran University of Science and Technology

Automotive Science and Engineering

Journal Homepage: ase.iust.ac.ir

ISSN: 2008-9899

Estimation of dynamic characteristics for fault detection of passive rubber engine mounts using continuous wavelet transform

Abbas Soltani *

Department of Industrial, Mechanical and Aerospace Engineering, Buein Zahra Technical University, Iran

ARTICLE INFO

Article history:
Received : 13 Jan 2026
Accepted: 15 Aug 2026
Published: 18 Sep 2026

Keywords:
Estimation
Dynamic characteristics
Hysteresis damping
Rubber engine mount
Continuous wavelet transform

A B S T R A C T

In this paper, a new method based on continuous wavelet transform (CWT) is presented to estimate the dynamic characteristics of the passive rubber engine mount (PREM), including the damped natural frequency and hysteretic damping ratio (HDR). The results of this research can be used to develop the technology and the experimental tests such as modal analysis to describe the behavior of hyperelastic materials in reducing noise transmission, vibrations and shock vibrations in resonance. The PREM will creep under the action of long-term load. Creep will change its original structure, resulting in changes in dynamic characteristics such as dynamic stiffness and HDR. These changes, which are often incremental and can also be caused by long-term storage by auto parts manufacturers, are considered as damage in PREMs. Hence, in this work, fault diagnosis in the PREMs in two cases of 25% and 55% increase in stiffness and hysteretic damping factor is also investigated using CWT. A single degree-of-freedom vibrating system subjected to an impulse input is modeled for the PREM. First, the energy distribution of the acceleration signal using the Morlet-based CWT is applied to determine the damped natural frequency of the system. Then, its HDR is estimated from the slope of the line obtained by plotting the cross-section for the logarithm of the CWT against time. By comparison of the estimated parameters and actual values, it can be concluded that the presented approach is highly accurate and efficient to estimate the dynamic properties of the PREM.

1. Introduction

In general, vibration isolators are devices for decreasing the magnitude of oscillations and the force transmitted from a vibrating base to equipment (or vice versa) in both the time and frequency domains. Vibration isolators have been widely used in industry, and efforts are ongoing to develop new applications to achieve higher performance. The passive rubber engine mount (PREM) is considered one of such isolators. The PREMs are one of the key components in powertrain systems that play an

*Corresponding Author
Email: soltani@bzte.ac.ir
http://doi.org/10.22068/ase.2026.747

"*Automotive Science and Engineering*" is licensed under a Creative Commons Attribution-Noncommercial 4.0 International License.

[Downloaded from ijae.iust.ac.ir on 2026-11-04]

important role in improving the noise, vibration and the harshness (NVH) quality of the vehicles. Researchers applied the nonlinear vibration analysis methods to optimize the PREM under harmonic base excitation having nonlinearity in both damping and stiffness. They have tended to use the analysis of nonlinear vibrations for isolation of the PREM for several reasons. For a most simplified case, the dynamic properties of an optimized PREM should vary with the excitation frequency to provide a hard PREM at frequencies higher than the natural frequency of the isolator and a soft PREM at frequencies lower than the natural frequency [1].

In reference [2], the application of nonlinear finite element method (FEM) was investigated to the identification of parameters for the passive hydraulic engine mounts. Utilizing hyperelastic materials, the fundamental relations of the incompressible nature of the rubber materials that constitute the main part of the engine mount were precisely described. The results of such research were directly used in lumped parameter models to give a thorough description of the dynamic behavior of two different hydraulic engine mounts. Zheng et al. designed a new passive engine mount which their performance depended on periodically distributed viscoelastic inserts.

A theoretical model was developed to describe the wave propagation dynamics in the new mount as well as a mechanical filter to prevent vibration propagation in specific frequency bands called the 'Stop Bands'. The model was built using Hamilton's principle using FEM theory combined with the transfer matrix method. A cell of the periodic mount was divided into four elements, and the transfer matrix formula for each element was given. The overall transfer matrix of the unit cell was found by multiplying the transfer matrices of the four elements constituting the cell [3-4].

Researchers investigated the adjustment of the stiffness coefficient of a passenger car engine mount in order to decrease the transmitted vibration to the driver according to the allowable values of natural frequencies for the engine utilizing the design of experiments (DOE) method. Based on previous experiments, common criteria have been presented by automobile manufacturers that lead the designer to the optimal values of the stiffness of the engine mount. In the aforementioned study, permissible frequency regions are determined by authoritative references on the NVH. To achieve this goal, combined FEM and multi-body dynamic modeling was used in the MSC/Nastran and Adams software, [5]. Rubber materials are used in rubber bushings of the chassis, gearbox, drive shaft and various parts of the suspension system connected to the body. In all these cases, their main role is to reduce the transmitted vibrations from the engine and gearbox to the body, improve the ride comfort and decrease the vibrations caused by road roughness. It is obvious that the NVH level of the vehicles can be greatly improved with detailed design of rubber bushings and elastomeric mounts assembled in the vehicle chassis [6].

Generally, the engine mounts have four main functions: (1) They support the dead weight of the engine and transmission system, (2) They control the vibrations and shocks caused by the displacement of the engine and the transmission system during sudden acceleration or braking, (3) They control the motion of the powertrain caused by low-frequency excitations from road irregularities. Low-frequency excitations are the harmonic oscillations with a frequency of less than 20 Hz. (4) Engine mounts isolate vibrations transmitted to the chassis from high-frequency excitations of the engine caused by combustion pulses and rotating parts into the engine during idling or cruising. For example, in a four-cylinder, four-stroke engine, the excitations caused by the engine's idling speed from 600 rpm to the maximum speed of 6000 rpm is pertinent to harmonic vibrations that vary in the frequency range of 20 to 200 Hz [7]. In the existing theories of torque roll axis decoupling, it is assumed that a rigid base for the powertrain mounting systems. Therefore, the effect of dynamic interaction between the powertrain and other subsystems is ignored. To cope with this shortcoming, a coupled mounting system problem is developed based on the linear time-invariant system theory [8].

A combined and approximate method based on FEM and experimental modeling is designed

[Downloaded from ijae.iust.ac.ir on 2026-11-04]

to analyze the dynamic properties of a rubber mounting. The hyperelastic-viscoplastic model is used to find the hysteresis of the rubber bushing in the FEM. In the experimental model, a spring, fractional derivatives, and friction elements are used to determine the dynamic stiffness of the rubber bushing over a wide range of excitation frequencies and amplitudes. The parameters of the presented empirical model are found utilizing the hysteresis curves determined from the FEM [9]. The researchers investigated an algorithm to choose a proper material model for a polyurethane rail pad. The selected material was presumed to be hyperelastic, and the model was chosen only using Mooney–Rivlin (M-R) material models. Also, a wide view of the selection process for hyperelastic material coefficients was indicated [10]. Improvement and optimization of the engine mount is one of the methods to enhance the NVH performance of the vehicle. In a study, the optimal stiffness coefficients for each of the engine mounts in three longitudinal, lateral and vertical directions were obtained so that the natural frequencies of the system remain constant and away from the excitation frequencies to prevent the resonance phenomena. The optimal stiffness coefficients were computed through the modal uncoupling theory based on the kinetic energy matrix [11]. In another reference, researchers represented the methods to determine the dynamic properties of a hyperelastic material, including the HDR and dynamic stiffness. It depended on the operating conditions, vibration theory and the frequency response function (FRF) diagrams. These methodologies can be extended to describe any type of hyperelastic material [12]. The general technical methods were introduced to develop the rubber-based and hyperelastic mounts for windmills. In addition, the issue of rubber life-time was explained, both theoretical and experimental. Also, the dynamical analysis of vibrational components for power generators, such as rubber mounts, was performed [13].

The experimental and numerical modal analysis of a mount bracket for the compressor was presented. The dynamic behavior of the mount bracket was studied using an impact test. The three-dimensional finite element models were developed through Altair HyperMesh and afterwards, a numerical modal analysis was carried out to find the natural frequencies and mode shapes in three-orthogonal directions [14]. The elastomeric angular mounts were applied as vibration dampers where vibration and its effective control are greatly important for the machinery structures. Furthermore, this experimental setup could be used to describe other polymeric damping materials. It was shown the dynamic stiffness and damping of such engine mounts were dependent on the frequency and vibration amplitude [15]. An approach was presented to optimize the geometry of the elastomer-based engine mount model utilizing topology optimization by taking their frequency-dependent nonlinear material properties. The method is based on an FEM engine mount model with obtaining a nonlinear FRF [16].

The experimental data showed that the stiffness of rubber aged for different times initially reduces and then increases with increasing temperature. The critical transition temperature reduces with increasing aging time. Moreover, the stiffness of rubber increases approximately linearly with aging time at different temperatures [17]. In fact, creep may cause stiffness reduction and relaxation or asynchronous changes. Also, creep causes stiffness change and damping change separately. But in this study, the hardness change model due to creep is based on the findings of the reference [17]. The measurement by means of hysteresis loops methodology is conducted for distinctive frequency and exerted force. The stiffness varies non-linearly during exciting in the range of natural frequency. The non-linearity in the PREM will not be significant if the excitation frequency increases [18]. The PREM will creep under the long-term loading. Creep will change its main structure, resulting in variations in static and dynamic properties and fatigue life. To cope with the issue of rubber engine mount creep, it was investigated the effect of creep properties on engine mount stiffness. For this, the mount creep was modeled theoretically based on the creep mechanism of rubber. The effects of different loads on the creep characteristics of engine mount were studied. The static viscoelastic

[Downloaded from ijae.iust.ac.ir on 2026-11-04]

parameters, loading intensity and creep analysis of rubber mount were studied [19]. An article was presented to research on static and dynamic properties of flexible mounts for investigation of their effects. Tension, compression, and shear experimental tests were conducted under quasi-static loading conditions to find stress-strain cycle curves. An overview of the Yeoh hyperelastic model including three parameters and discussion on the calibration of these parameters was indicated for description of the hyperelastic material characteristic [20].

The main parameters of design, consisting of structural rigidity, damping, and thermal effects were studied utilizing the FEM and multi-objective optimization approaches in electric vehicles. In addition, the research takes into account lightweight materials and damping properties to minimize the NVH at the same time as making sure the mechanical stability [21].

Since the hysteresis damping factor and the stiffness of the rubber engine mounts play a significant role to reduce the transmitted vibration to the vehicle body, it is of fundamental importance to estimate the dynamic characteristics of PREM. Regarding the review of past studies, there is little literature about estimation methods for the dynamic properties of rubber mounts. However, in the reference [12], the HDR and dynamic stiffness was obtained by using the FRF based on hardware and software laboratory equipment for frequency analysis. While the parameter estimation method in this article is utilizing the CWT of the impulse response, only the accelerometer sensor and a modal hammer equipped with a force sensor will be applied in the experimental equipment for practical implementation. As a result, compared to the algorithm indicated in [12] and other previous research, the dynamics characteristics will be identified in a more cost-effective way in this paper, and also according to the results of parameter identification and fault detection of rubber mounts, its high accuracy can be concluded. These are two major technical contributions of this study.

Accordingly, in the second part of the paper, a single degree-of-freedom (SDOF) dynamic model of PREM with hysteresis damping is explained. Then, the theory of CWT is presented in the third part. In the next section, the estimation approach using Morlet-based CWT is proposed. The performance of the presented method to estimate the dynamic characteristics and diagnose the damages of PREM is discussed with simulation in the fifth part. Finally, the conclusions are listed in the sixth part.

2. Dynamics model of the PREM

An equivalent SDOF dynamic model of PREM is illustrated in Figure 1 to give a better demonstration of translational mount motion. This model is used in vibration testing to estimate the dynamic characteristics of rubber mounts. The practical and realistic model in a vehicle includes the base motion.

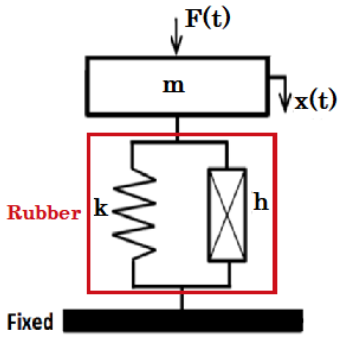


Figure 1: An equivalent SDOF dynamic model of the PREM

The equation of motion can be expressed as follows:

$$m\ddot{x} + k^*x = F(t) \quad (1)$$

$$k^* = k + ih = k\,(1 + ig) \quad (2)$$

$$g = \frac{h}{k} \quad (3)$$

where, k^* is from equation (2) should be replaced in equation (1). Therefore, the dynamic equation of the system can be derived by the following expression:

$$m\ddot{x} + kx + igkx = F(t) \quad (4)$$

In the above equations, k is the dynamic elastic constant, h is the hysteretic damping coefficient, m is the mass of mount excited by an

[Downloaded from ijae.iust.ac.ir on 2026-11-04]

input force $F(t)$ and oscillating with amplitude $x(t)$ and, g is the hysteretic damping factor of the rubber.

3. Continuous wavelet transform

The CWT is based upon a family of functions [22]:

$$\psi_{a,b}(t) = \frac{1}{\sqrt{a}}\psi\left(\frac{t-b}{a}\right), \quad a > b \in \mathcal{R} \tag{5}$$

where, ψ is a fixed function, called the 'mother wavelet', which is localized both in time and frequency. The function $\psi_{a,b}(t)$ is obtained by applying the operations of shifting (b-translation) in the time domain and scaling (a-dilation) in the frequency domain to the mother wavelet. In this study, the Morlet wavelet is used by central frequency $f_o = 0.8125\ Hz$. The CWT of a signal x(t) is computed by

$$W_x^{\psi}(a,b) = \int_{-\infty}^{\infty} x(t)\psi_{a,b}^{\star}(t)dt = \frac{1}{\sqrt{a}}\int_{-\infty}^{\infty} x(t)\psi^{\star}\left(\frac{t-b}{a}\right)dt \tag{6}$$

where, $\psi^*(t)$ is the complex conjugate of $\psi(t)$. The relationship between the scale parameter a and signal frequency f_a can be found as, [22]:

$$f_a = \frac{f_o}{a} \tag{7}$$

In the CWT obtained by MATLAB software, the relationship between the values of the vertical axis in the time-scale contour (a_{MAT}) and the scale a is expressed as follows in which, f_{samp} is the sampling frequency.

$$a = \frac{a_{MAT}}{f_{samp}} \tag{8}$$

By combining the equations (7) and (8):

$$f_a = \frac{f_o \cdot f_{samp}}{a_{MAT}} \tag{9}$$

3.1. Scalogram

The contribution of signal energy in the scale a, and the translation b, is given by two-dimensional wavelet energy density function known as the scalogram.

$$E(a,b) = \left|W_x^{\psi}(a,b)\right|^2 \tag{10}$$

The total signal energy distribution in the scale a is obtained as, [22]:

$$E(a) = \int_{-\infty}^{\infty} E(a,b)db \tag{11}$$

The unit of CWT for the acceleration signal is $(\frac{m}{s^2})$. So, the dimensions of $E(a,b)$ and $E(a)$ will be $(\frac{m}{s^2})^2$.

4. Estimation of dynamic characteristics based on the CWT

The characteristic equation of system described by equation (4) can be expressed as follows

$$ms^2 + k\,(1+ig) = 0 \tag{12}$$

The roots of characteristic equation are obtained by the following expression in which, $\omega_n = \sqrt{k/m}$.

$$s_{1,2} = \pm\omega_n\sqrt{1+ig}\ \ i \tag{13}$$

According to the formula for square roots of the complex numbers:

$$s_{1,2} = -\omega_n\zeta_h \pm \omega_d\, i \tag{14}$$

$$\zeta_h = \sqrt{0.5(\sqrt{1+g^2}-1)} \tag{15}$$

$$\omega_d = \omega_n\sqrt{1+\zeta_h^2} \tag{16}$$

In the above equations, ω_n and ω_d are the undamped and damped natural frequency respectively and, ζ_h is the HDR corresponding to the hyperelastic materials. The impulse response of the SDOF dynamic system of

[Downloaded from ijae.iust.ac.ir on 2026-11-04]

PREM illustrated in Figure 1 can be expressed as

$$x(t) = X.e^{-\zeta_h \omega_n t}.sin(\omega_d + \phi) \quad (17)$$

where, X is the residue magnitude and ϕ is the phase angle. First, an analytic form of signal $x(t)$ depicted by $\hat{x}(t)$, should be found by Hilbert transform [23]:

$$\hat{x}(t) = x(t) + jx_H(t) \quad (18)$$

$$x_H(t) = \int_0^{\infty} \frac{x(\tau)}{t-\tau}\, d\tau \quad (19)$$

The analytic form for the impulse response of the system, equation (17), assuming a low damping ratio:

$$\hat{x}(t) = X.e^{-\zeta_h \omega_n t}.e^{-j\omega_d t + \phi} \quad (20)$$

Presuming that the envelope of the system response varies slowly, the Morlet-based CWT of $\hat{x}(t)$ can be given as follows:

$$W_x^{\psi}(t,\omega) = \sqrt{2\pi \frac{\omega_0}{\omega}} X.e^{-\zeta_h \omega_n t}.e^{j\omega_d t}.e^{-\frac{1}{2}\omega_0^2 [(\frac{\omega_d}{\omega})-1]^2} \quad (21)$$

where, $\omega_0 = 2\pi f_0$. Assuming the damped natural frequency, ω_d, is well separated in frequency, in comparison with ω_0, modal contributions in the CWT will be distinct. In this case, for a fixed value of frequency $\omega = \omega_d$, the logarithm of the CWT can be approximated as

$$ln\left|W_x^{\psi}(t,\omega)\right| \approx -\omega_n \zeta_h t + \ln\left|X\sqrt{2\pi \frac{\omega_0}{\omega_d}}\right| \quad (22)$$

According to the time-scale contour of the CWT of the impulse response of the system, a dominant frequency is revealed as light spot that indicate the damped natural frequency of the rubber mount. Afterwards, the frequency related to the bright spot is computed using equation (9). Then, from equation (22), the HDR of the system, ζ_h, can be estimated using the slope of the line approximated by plotting the cross-section for the logarithm of absolute value of the CWT against time. A measurement zero-mean white noise is added to the acceleration diagram to make the simulation results closer and more similar to the laboratory conditions. The impulse response of the

5. Simulation results

In order to evaluate the presented method, the parameters of the PREM are shown in Table 1. The sampling frequency f_{samp} is $2000\ Hz$. The system is exposed to an impulse of $0.002\ Ns$. Using the parameters values, the theoretical values of the HDR and damped natural frequency are calculated through equations (15) and (16) and are tabulated in Table 1. A measurement zero-mean white noise is added to the acceleration diagram to make the simulation results closer and more similar to the laboratory conditions.

5.1. Parameter estimation

To estimate the parameters, the system excited under the impulse input. The impulse response of the PREM in the time interval of zero to $0.1\ s$ is illustrated in Figure 2. In the Figure 3, the time-scale contour of the acceleration is depicted. Taking into account the sampling frequency is $2000\ Hz$, the relation between dimensionless coefficient b and time t can be found as follows:

$$t = \left(\frac{1}{f_{samp}}\right).b = 5 \times 10^{-4}\ (sec)\ .b \quad (23)$$

Thus, the final b, b_{fin}, can be computed as

[Downloaded from ijae.iust.ac.ir on 2026-11-04]

$$b_{fin} = t_{fin} . f_{samp} = 0.1 \times 2000 = 200 \qquad (24)$$

The values of a and b are dimensionless parameters. Therefore, the values on the horizontal axis in Figure 3 should be multiplied by 5×10^{-4} (sec).

In Figure 3, a dominant frequency is observed as center of light contour. For this signal, the energy distribution $E_{(a)}$, equation (11), is shown in Figure 4 to find the dominant frequency, precisely.

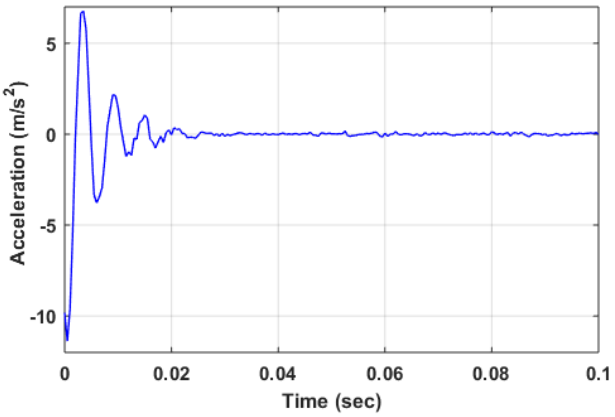


Figure 2: Impulse response of the PREM

Table 1: Parameter values of the PREM model [24]

Parameter	Unit	Value
$Mass$	kg	0.167
$Dynamic\ Elastic\ Constant$	KN/m	195.2
$Hysteretic\ Damping\ Factor$	–	0.326
$Hysteretic\ Damping\ Ratio\ (Theory)$	–	0.161
$Damped\ Natural\ Frequency\ (Theory)$	Hz	174.3

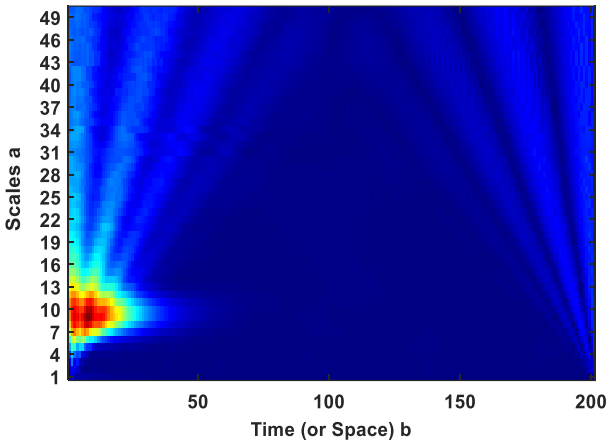


Figure 3: CWT of acceleration signal to the impulse input

According to Figure 4, the pick scale of acceleration signal is equal to 9. Equation (9) is utilized to obtain the corresponding frequency in any scale such that the frequency can be substituted for the scale values concerning the horizontal axis of Figure 4. For instance, the damped natural frequency of the PREM can be calculated as follows:

$$\omega_d = \left(\frac{0.8125 \times 2000}{9}\right).2\pi = 1134.1\ (\frac{rad}{s}) \qquad (25)$$

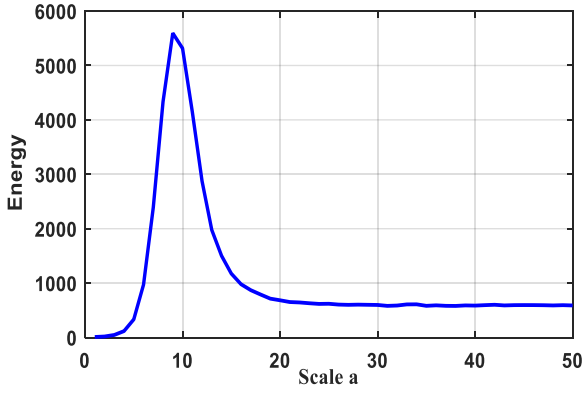


Figure 4: Energy distribution of Acceleration signal using CWT

According to the equations of (16) and (25):

$$\omega_n \sqrt{1 + \zeta_h^2} = 1134.1 \qquad (26)$$

[Downloaded from ijae.iust.ac.ir on 2026-11-04]

By plotting the cross-section for the logarithm of absolute value of the CWT corresponding to scale $a = 9$ against time, Figure 5, the slope of the line will be approximated to $-\omega_n\zeta_h$. For this reason, two points $P_1 = (0.012, 2.0333)$and $P_2 = (0.03, -1.0771)$ are considered and the slope of the line passing through two points is obtained base on equation (26) and then, the line is plotted in Figure 5. The remarkable fit of the tangent to the logarithm of CWT coefficients in Figure 5 represents that the logarithmic curve is straight.

$$-\omega_n\zeta_h = \frac{\Delta y}{\Delta x} = \frac{2.0333 + 1.0771}{0.012 - 0.03} \Longrightarrow$$
$$\omega_n\zeta_h = 172.8 \tag{27}$$

By solving the equations of (26) and (27), two unknowns ω_n and ζ_h are derived and then listed in Table 2. The theoretical values of damped natural frequency and HDR obtained using actual values of the parameters are shown in Table 2. In addition, the estimated results of dynamic characteristics of the PREM based on CWT are listed. As shown in Table 2, the high effectiveness of the presented method can be concluded to estimate the dynamic properties of the PREM without noticeable errors. The errors of estimation for the damped natural frequency and HDR are 3.6% and 4.3%, respectively.

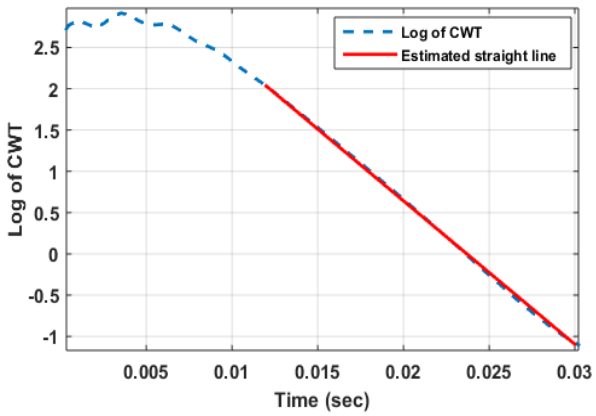


Figure 5: Cross-section for the logarithm of the CWT for scale $a = 9$ ($f_d = 180.5\ Hz$)

Table 2: Estimation results of dynamic characteristics for the PREM

Parameter	Unit	Theory	Estimated	Error (%)
Damped Natural Frequency	*Hz*	174.3	180.55	3.6
Hysteretic Damping Ratio	–	0.161	0.154	4.3

5.2. Fault detection

Similar to the previous part, the system is excited under the impulse input to detect the faulty PREM. The time interval of input is zero to $0.1\ s$. Two different damage states in the rubber mount are assumed to be 25% and 55% increase in the hysteretic damping factor and dynamic stiffness. These damages can be caused by creep due to long-term operation or long-term storage by automotive parts manufacturers.

The time-scale contours of the acceleration by CWT for faulty state 2 is observed in the Figure 6. To detect the damaged mount, the energy value of the acceleration signal in any scale is used to find the damped natural frequency of the system. For this, $E_{(a)}$ from equation (11) is used for the acceleration signal in three states: normal mount, damaged mount with a 25% increase in the hysteretic damping factor and dynamic stiffness (faulty state 1), and damaged mount with a 55% increase in the aforementioned parameters (faulty state 2), as shown in Figure 7.

Again, equation (9) is applied to relate the pick scale of energy signal and the corresponding frequency, ω_d. Then, by determining the slope of straight line in the cross-section for the logarithm of absolute value of the CWT related to the scale of pick, Figure 8, the $-\omega_n\zeta_h$ value is found. Afterwards, by solving the equations of (16) and the known value of $-\omega_n\zeta_h$, two unknowns ω_n and ζ_h are calculated. Finally, the dynamic elastic constant, k, is obtained from the equation $\omega_n = \sqrt{k/m}$. The estimation results are illustrated in Table 3.

According to Table 3, the acceleration signal energy in faulty states 1 and 2 has significantly

[Downloaded from ijae.iust.ac.ir on 2026-11-04]

decreased by 31.2% and 53.3%, respectively, compared to the normal state. The main reason for this is the increase in the hysteretic damping factor by 25% and 55%, respectively.

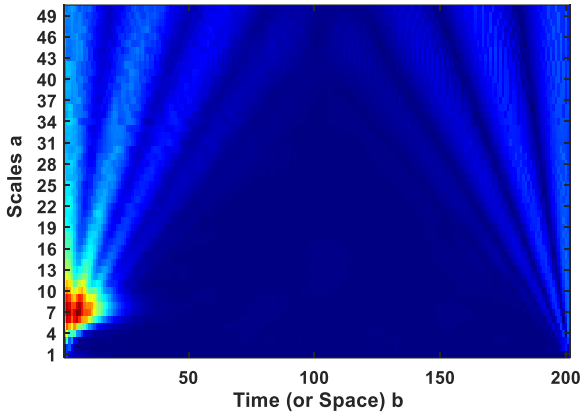


Figure 6: CWT of acceleration signal to the impulse input for faulty state 2

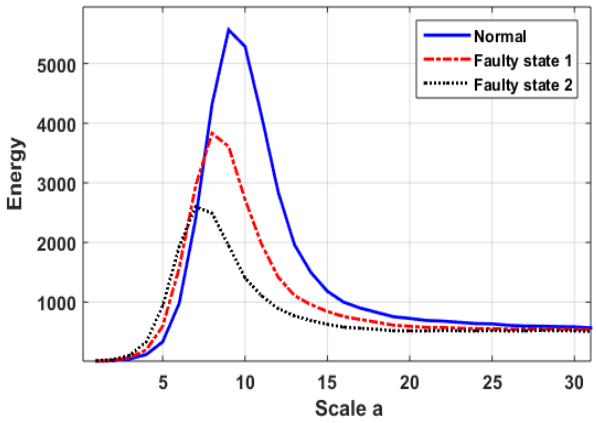


Figure 7: Comparison between energy distribution for acceleration of PREM in normal condition, faulty state 1 and faulty state 2 using CWT

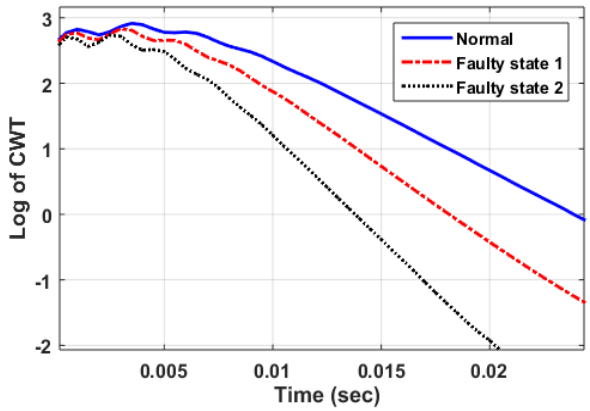


Figure 8: Comparison between Cross-section for the logarithm of the CWT in normal condition, faulty state 1 and faulty state 2

Also, in the faulty states 1 and 2, the damped natural frequency of the system has a noticeable increase by 12.5% and 28.5%, respectively, compared to the undamaged state. It is mainly due to increasing the stiffness of the system. In addition, the hysteretic damping ratio has also increased considerably by about 24.6% and 54.5% in the first and second damaged states. As is expected, the remarkable amount of change in the damping ratio is observed, which is due to the increase in the hysteresis damping factor of the rubber because of the creep.

It should be noted the results presented in this paper are based on analysis and simulation. According to the precise results obtained, as well as the author's previous research involving laboratory testing and wavelet transform for fault diagnosis in suspension system components [22], the necessary laboratory equipment has been prepared to evaluate the proposed method. This could be addressed as a topic for future research in the next paper. Real data from a faulty mount can also be used in the same future work.

[Downloaded from ijae.iust.ac.ir on 2026-11-04]

Table 3: Estimation results of dynamic characteristics for the PREM in normal condition, faulty state 1 and faulty state 2

Parameter	Unit	Normal	Faulty State 1	Faulty State 2
Pick scale	–	9	8	7
Maximum Energy	$m^2.Hz$	5566	3830	2600
Line Slope of logarithmic curve	rad/s	−172.8	−240	−338
Damped Natural Frequency	Hz	180.55	203.1	232.1
Hysteretic Damping Ratio	–	0.154	0.192	0.238
Natural Frequency	Hz	178.58	198.94	226.03

6. Conclusion

This paper presented a method based on CWT to estimate the dynamic characteristics of the PREM, including the damped natural frequency and the HDR. In addition, the damage diagnosis in the PREM in two cases of 25% and 55% increase in stiffness and hysteretic damping factor was also investigated using CWT. A SDOF system subjected to the impulse input was modeled for the PREM. The energy distribution of the acceleration signal utilizing the Morlet-based CWT was applied to obtain the damped natural frequency of the system. Afterwards, the HDR was estimated from the slope of the line obtained by plotting the cross-section for the logarithm of the CWT against time. The errors of estimation for the damped natural frequency and HDR were 3.6% and 4.3%, respectively. By comparison of the estimated parameters and actual values, it can be found that the presented method may estimate the dynamic properties of the PREMs, accurately and detect the faulty rubber mounts, precisely.

References

[1] A. Narimani, M. F. Golnaraghi, G. Nakhaie Jazar. Dynamic behavior comparison of passive hydraulic engine mounts. Part 2: Finite element analysis. Journal of Vibration and control, Vol. 10, (2004), pp. 1775-1794.

[2] J. Christopherson, G. Nakhaie Jazar. Frequency response of a piecewise linear vibration isolator. Journal of Sound and Vibration, Vol. 290, No. 3, (2006), pp. 1071-1090.

[3] L. Zheng, W. Jung, Z. Gu, A. Baz. Passive periodic engine mount. International Design Engineering Technical Conferences and Computers and Information in Engineering Conference, Vol. 43291, (2008), pp. 607-612.

[4] W. Jung, Z. Gu, A. Baz. Mechanical filtering characteristics of passive periodic engine mount. Finite elements in analysis and design, Vol. 46, No. 9, (2010), pp. 685-697.

[5] A. Keshavarz, M. Bayani Khaknejad, S. Azadi. Improving vehicle NVH behavior via tuning the engine mount stiffness using doe method. SAE 2011 Noise and Vibration Conference and Exhibition 178661, (2011) May 17.

[6] Sh. Shaoliang, W. Weiwei, H. Hu, L. Xintian. The nonlinear finite element analysis and experimental study of rubber bushing. 2011 Third International Conference on Measuring Technology and Mechatronics Automation, IEEE, Vol. 3, No.2, (2011), pp. 870-873.

[7] M. Azadi, S. Behzadipour, G. Faulkner. Introducing a new semi-active engine mount using force controlled variable stiffness. Vehicle system dynamics, Vol. 51, No. 5, (2013), pp. 721-736.

[8] J. Fang Hu, R. Singh. Improved torque roll axis decoupling axiom for a powertrain mounting system in the presence of a compliant base. Journal of Sound and Vibration, Vol. 331, No. 7, (2012), pp. 1498-1518.

[9] H. Seong Lee, J. Kyong Shin, S. Msolli, H. Soo Kim. Prediction of the dynamic equivalent stiffness for a rubber bushing using

[Downloaded from ijae.iust.ac.ir on 2026-11-04]

the finite element method and empirical modeling. International Journal of Mechanics and Materials in Design, Vol. 15, No. 1, (2019), pp. 77-91.

[10] P. Szurgott, L. Jarzębski. Selection of a hyper-elastic material model-a case study for a polyurethane component. Latin American Journal of Solids and Structures, Vol. 16, (2019): e191.

[11] M. A. Porgoo, B. Mashadi, A. H. Kakaee. Powertrain mounting system optimization to improve vibration behavior of EF7 engine. The Journal of Engine Research, Vol. 53, (2019), pp. 55-68.

[12] M. Ciolca, D. Vlasceanu. Experimental analysis of hyperelastic materials using the vibration method. Materiale Plastice, Vol. 61, No. 2, (2024), pp. 117-128.

[13] T. Böhme, A. Padiosa, S. Woltera. Development and design of elastic, rubber-based mounts for different components of windmills: example and engineering backgrounds. Proceedings of WindEurope Summit, (2016) September, 27-30th, Hamburg (Germany).

[14] A. Meena, S. Sen, V. Suthar. Experimental and numerical modal analysis of a compressor mounting bracket. IOSR Journal of Mechanical and Civil Engineering, Vol. 14, No. 1, (2017), pp. 01-07.

[15] S. Kumar Battula, P. Rama Murty Raju, C. H. Ratnam. Engine isolation angular mount with different types elastomers. Materials Today: Proceedings, Vol. 5, No. 9, (2018), pp. 19555-19564.

[16] S. Bahr, G. Jacobs, G. Höpfner, E. Hensel, J. Troge, T. Rapp. Topology optimization of nonlinear elastomer engine mounts considering the transfer behavior. Forschung im Ingenieurwesen, Vol. 89, No. 1, (2025), pp. 72-81.

[17] Z. Xie, D. Jia, X. Huang, K. Zhang, S. Yan, J. Chen, J. Li, W. Zhong. Influence of temperature on hyperelastic mechanical behavior of accelerated aged EPDM rubber. Polymers, Vol. 17, No. 12, (2025), pp. 1626-1648.

[18] I. Zikrullah Zainudin, O. Lu Ean. Experimental identification on non linear properties of rubber mount. MATEC Web of Conferences, EDP Sciences, Vol. 217, (2018), p. 02007.

[19] J. Fu, Y. Liu, J. Su, B. Chen, Z. Chen. Rubber creep model and its influence on mounting stiffness. Applied Sciences, Vol. 12, No. 24, (2022), pp. 12764-12779.

[20] S. Ju Park, B. Park, J. Yeob Lee, Y. Ho Shin, C. Lim Jeong, S. Jae Kim, K. Kim. Study on dynamic characteristics of resilient mount under preload. Materials, Vol. 17, No. 20, (2024), pp. 5096-5110.

[21] S. Hazra, K. Janardhan Reddy. Design optimization of engine mounting system for a modular electric vehicle platform with different powertrain characteristics. Journal of Physics: Conference Series, Vol. 2198, No. 1, (2022), IOP Publishing, p. 012014.

[22] S. Azadi, A. Soltani. Fault detection of vehicle suspension system using wavelet analysis. Vehicle System Dynamics, Vol. 47, No. 4, (2009), pp. 403–418.

[23] S. K. Lee, P. R. White. Application of wavelet analysis to the impact harshness of a vehicle. Proceedings of the Institution of Mechanical Engineers, Part C: Journal of Mechanical Engineering Science, Vol. 214, , No. 11, (2000), pp. 1331-1338.

[24] Determining the dynamic characteristics of the engine mount of gearbox side for L90 passenger car using the frequency response function (FRF) diagram reported by the Research and Development group of Niromoharreke industrial (NMI) company.

[Downloaded from ijae.iust.ac.ir on 2026-11-04]